Novel Intercalation Host System Based on Transition Metal (Fe^{2+}, Co^{2+}, Mn^{2+})−Chloranilate Coordination Polymers. Single Crystal Structures and Properties

Satoshi Kawata,[†] Susumu Kitagawa,*[,‡] Hitoshi Kumagai,[§] Tetsuya Ishiyama,[§] Kenji Honda,[§] Hiroshi Tobita,[§] Keiichi Adachi,[†] and Motomi Katada[§]

Department of Chemistry, Shizuoka University, Shizuoka 422-8529, Japan, Department of Synthetic Chemistry and Biological Chemistry, Graduate School of Engineering, Kyoto University, Yoshida, Sakyo-ku, Kyoto, 606-8501, Japan, and Department of Chemistry, Tokyo Metropolitan University, Hachioji 192-0397, Japan

Received May 5, 1998. Revised Manuscript Received September 14, 1998

The new iron(II), cobalt(II), and manganese(II) intercalation compounds $\{[M(CA)(H_2O)_2]\cdot(G)\}_n$ (M = Fe^{2+}, Co^{2+}, Mn^{2+}; H_2CA = chloranilic acid ($C_6H_2O_4Cl_2$); G = H_2O and phenazine ($C_{12}H_8N_2$; phz)) have been synthesized and characterized. $\{[Fe(CA)(H_2O)_2](H_2O)\}_n$ (**1a**) crystallizes in the monoclinic space group *C*2/*c* (No. 15) with $a = 4.914(2)$ Å, $b = 14.222(2)$ Å, $c = 13.987(2)$ Å, $\beta = 94.98(2)°$, $V = 973.8(4)$ Å^3, and $Z = 4$. $\{[Fe(CA)(H_2O)_2](phz)\}_n$ (**2a**) crystallizes in the triclinic space group $P\bar{1}$ (No. 2) with $a = 8.079(2)$ Å, $b = 11.366(3)$ Å, $c = 5.055(2)$ Å, $\alpha = 96.57(3)°$, $\beta = 98.70(3)°$, $\gamma = 83.07(2)°$, $V = 453.3(3)$ Å^3, and $Z = 1$. $\{[M(CA)\cdot(H_2O)_2](H_2O)\}_n$ (M = Co^{2+} (**1b**), Mn^{2+} (**1c**)) are isomorphous to **1a**. For **1a**−**c**, crystal structures consist of uncoordinated guest water molecules and one-dimensional zigzag $[M(CA)(H_2O)_2]_k$ chains. Two water molecules occupying cis positions and two chloranilate filling the remaining sites in a bis bidentate fashion create the octahedral environment around the metal ion to form a zigzag chain (type I), which extends along the diagonal between the *a* and *c* axes. The adjacent chains are interlinked by hydrogen bonds, thus forming layers, which spread out along the *ac* plane. Water molecules are intercalated between the $\{[M(CA)(H_2O)_2]_k\}_l$ layers. The intercalation mode of the water molecules is different from those in $\{[M(CA)(H_2O)_2](phz)\}_n$ (M = Fe^{2+} (**2a**), Co^{2+} (**2b**), Mn^{2+} (**2c**)), which are isomorphous each other. The crystal structures of **2a**−**c** consist of uncoordinated phenazine molecules and straight $[M(CA)(H_2O)_2]_k$ chains (type II). Infinite, nearly coplanar linear chains are formed by metal ions and the bis-chelating CA^{2-} anions, which extend along the *a* direction, and are linked by hydrogen bonds between the coordinated water and the oxygen atoms of the CA^{2-} on the adjacent chains, forming a two-dimensional sheet, which spreads out along the *ac* plane. The intercalated phenazines are stacked along the *c* axis perpendicular to the $[M(CA)(H_2O)_2]_k$ chain, and the planes of the phenazine molecules are tilted to the stacking direction, forming a segregated columnar structure between the $\{[M(CA)(H_2O)_2]_k\}_l$ layers. The ^{57}Fe Mössbauer spectra of **1a** and **2a** consist of a single quadrupole doublet with $IS = 1.16$ mm/s (**1a**), 1.16 mm/s (**2a**) and $QS = 2.53$ mm/s (**1a**), 1.46 mm/s (**2a**) at 298 K, indicating that the oxidation state of the iron in both complexes is two. The magnetic susceptibilities were measured from 2 to 300 K and analyzed by a one-dimensional Heisenberg-exchange model to yield $J = -0.74$ cm^{-1}, $g = 2.01$, $\rho = 1.4\%$ (**1c**) and $J = -0.65$ cm^{-1}, $g = 2.02$, $\rho = 9.0\%$ (**2c**).

Introduction

Building transition metal complex-based layered compounds[1−6] is an important step to create a system which would provide cooperative conductive[7−12] and magnetic properties.[13−19] Self-assembly processes[20−22]

[†] Shizuoka University.
[‡] Kyoto University.
[§] Tokyo Metropolitan University.

(1) *Organic and Inorganic Low Dimensional Crystalline Materials*; Delhaes, P.; Drillon, M., Eds.; D. Reidel: Dordrecht, The Netherlands, 1987.
(2) *Magnetic Molecular Materials*; Gatteschi, D., Kahn, O., Miller, J. S., Palacio, F., Eds.; D. Reidel: Dordrecht, The Netherlands, 1991.
(3) *Inorganic Materials*, 2nd ed.; Bruce, D. W., O'Hare, D., Eds.; John Wiley & Sons: New York, 1996.
(4) *Magnetism: A Supramolecular Function*; Kahn, O., Ed.; Kluwer: Dordrecht, The Netherlands, 1996.
(5) Burrows, A. D.; Chang, C. W.; Chowdhry, M. M.; McDrady, J. E.; Mingos, D. M. P. *Chem. Soc. Rev.* **1995**, 329.
(6) Kawata, S.; Kitagawa, S.; Kumagai, H.; Kudo, C.; Kamesaki, H.; Ishiyama, T.; Suzuki, R.; Kondo, M.; Katada, M. *Inorg. Chem.* **1996**, *35*, 4449.
(7) Gómez-García, C. J.; Ouahab, L.; Gimenez-Saiz, C.; Triki, S.; Coronado, E.; Delhaès, P. *Angew. Chem., Int. Ed. Engl.* **1994**, *33*, 223.
(8) Kurmoo, M.; Graham, A. W.; Day, P.; Coles, S. J.; Hursthouse, M. B.; Caulfield, J. L.; Singleton, J.; P., F. L.; Hayes, W.; Ducasse, L.; Guionneau, P. *J. Am. Chem. Soc.* **1995**, *117*, 12209.
(9) Clemente-León, M.; Mingotaud, C.; Agricole, B.; Gómez-Garcia, C. J.; Coronado, E.; Delhaès, P. *Angew. Chem., Int. Ed. Engl.* **1997**, *36*, 1114.
(10) Clemente-León, M.; Coronado, E.; Galán-Mascarós, J.-R.; Gómez-García, C. J. *J. Chem. Soc., Chem. Commun.* **1997**, 1727.

10.1021/cm980326v CCC: $15.00
Published on Web 11/06/1998

offer a particularly attractive approach for preparing such entities.[23−32] Especially, the generation of arrays by metal ions and organic guest molecules is interesting in this respect, as the presence of guest molecules may endow the resulting organic−inorganic hybrid architecture with novel redox, optical, magnetic, and other properties enhanced by host−guest interaction.[6,33−38]

Very recently, taking advantage of the strong hydrogen-bonding ability of the pyridine-hydroxyl group and oxocarbon-hydroxyl group, we prepared some novel intercalation compounds which consist of the straight 1-D chain $[M(CA)(H_2O)_2]_k$ ($M = Cu^{2+}$, H_2CA = chloranilic acid ($C_6H_2O_4Cl_2$)) and uncoordinated guest molecules.[6] The chains are linked by hydrogen bonds between the coordinated water and the oxygen atoms of the CA^{2-} anion on the adjacent chain, forming layers. The guest molecules are intercalated between the $\{[Cu(CA)(H_2O)_2]_k\}_l$ layers, which are supported with the N- -H_2O hydrogen bonding. The layers are so flexible that various sizes of guest molecules can be intercalated between the layers together with the columnar stack formed. The extension of this chemistry would afford new materials if the common layers are constructed by other metals and intercalate organic molecules with functionalities such as conducting and/or photosensitized properties.

On the other hand, the polyoxocarbon molecules have frontier orbitals with energies comparable to those of the transition metal ions and the nature of the reduced and oxidized species depends on the metal ions and the coordination environment. Examples from this class of compounds include $[M_2(CTH)_2(DHBQ)]^{3+}$ (M = Cr(III) or Fe(III); CTH = *dl*-5,7,7,12,14,14-hexamethyl-1,4,8,-11-tetraazacyclotetradecane; H_2DHBQ = dihydroxybenzoquinone ($C_6H_4O_4$))[39] and $(Bu_4N)_2[Mo_4O_{10}(DHBQ)_2]$.[40] The existence of the compound $[M_2(CTH)_2(DHBQ)]^{3+}$ demonstrated that radical species can be stabilized with iron and chromium. The DHBQ radical behaves as a linking ligand, which can yield reasonably strong antiferromagnetic coupling with the metals. Moreover, a mixed valence iron coordination polymer with DHBQ was obtained by solid-state I_2 oxidation.[41,42] The background of this chemistry also prompts us to construct new layer compounds by using redox active metals such as iron and DHBQ derivatives.

To develop the intercalation chemistry of the metal−chloranilate system toward new functional materials, we describe here the common intercalation structures constructed from one-dimensional coordination polymers and guest molecules, $\{[M(CA)(H_2O)_2](G)\}_n$ ($M = Fe^{2+}$, Co^{2+}, Mn^{2+}; G = H_2O and phenazine ($C_{12}H_8N_2$; phz)). In the case of G = H_2O, the compounds consist of zigzag chains (type I structure) and guest water molecules. On the other hand, the sheet structure is constructed by straight chains (type II) for G = phenazine. We discuss the factors that determine the chain and sheet structures. In addition to the crystal structures and magnetic properties, the thermal properties are also described.

Experimental Section

Syntheses of $\{[M(CA)(H_2O)_2](H_2O)\}_n$ (1a−c). ***1a.*** An aqueous solution (10 mL) of iron(II) sulfate heptahydrate (6×10^{-5} mol) was transferred to a glass tube, and then an aqueous solution (10 mL) of H_2CA (6×10^{-5} mol) was poured into the tube without mixing the two solutions under a nitrogen atmosphere. Dark gray plate crystals began to form in 1 week. One of these crystals was used for X-ray crystallography. Physical measurements were conducted on a polycrystalline powder that was synthesized as follows: An aqueous solution (100 mL) of H_2CA (6×10^{-4} mol) was added dropwise to a 6×10^{-4} mol amount of iron(II) sulfate heptahydrate dissolved in 20 mL of water under nitrogen atmosphere. Upon stirring of the mixture, the dark gray powder appeared immediately. Anal. Calcd for $FeCl_2O_7C_6H_6$: C, 22.74; H, 1.91. Found: C, 22.32; H, 1.90. IR (KBr pellet): 3424 vs, 2973 w, 1578 m, 1508 vs, 1381 s, 1314 w, 1009 m, 857 s, 774 w, 616 m, 603 m, 578 m cm^{-1}. The identification of batches for magnetic and single-crystal data collection has been confirmed by powder X-ray diffraction pattern (XRD). The XRD pattern of the powdered sample is in good agreement with the simulated pattern reproduced from the F_c values of the calculated crystal structure.

$\{[M(CA)(H_2O)_2](H_2O)\}_n$ ($M = Co^{2+}$ (**1b**), Mn^{2+} (**1c**)) were synthesized from cobalt(II) sulfate heptahydrate and manganese(II) chloride tetrahydrate, respectively, by a procedure

(11) Munakata, M.; Wu, L. P.; Yamamoto, M.; Kuroda-Sowa, T.; Maekawa, M. *J. Am. Chem. Soc.* **1996**, *118*, 3117.
(12) Munakata, M.; Wu, L. P.; Kuroda-Sowa, T. *Bull. Chem. Soc. Jpn.* **1997**, *70*, 1727.
(13) De Munno, G.; Ruiz, R.; Lloret, F.; Faus, J.; Sessoli, R.; Julve, M. *Inorg. Chem.* **1995**, *34*, 408.
(14) De Munno, G.; Poerio, T.; Viau, G.; Julve, M.; Lloret, F.; Journaux, Y.; Rivière, E. *J. Chem. Soc., Dalton Trans.* **1996**, 2587.
(15) Chen, Z. N.; Fu, D. G.; Yu, K. B.; Tang, W. X. *J. Chem. Soc., Dalton Trans.* **1994**, 1917.
(16) Umeya, M.; Kawata, S.; Matsuzaka, H.; Kitagawa, S.; Nishikawa, H.; Kikuchi, K.; Ikemoto, I. *J. Mater. Chem.* **1998**, *10*, 295.
(17) Inoue, K.; Hayamizu, T.; Iwamura, H.; Hashizume, D.; Ohashi, Y. *J. Am. Chem. Soc.* **1996**, *118*, 1903.
(18) Cortés, R.; Lezama, L.; Pizarro, J. L.; Arriortua, M. I.; Rojo, T. *Angew. Chem., Int. Ed. Engl.* **1996**, *35*, 1810.
(19) Lloret, F.; Munno, G. D.; Julve, M.; Cano, J.; Ruiz, R.; Caneschi, A. *Angew. Chem., Int. Ed. Engl.* **1998**, *37*, 135.
(20) Lehn, J.-M. *Supramolecular Chemistry: Concepts and Perspectives*; VCH: Weinheim, Germany, 1995.
(21) Kawata, S.; Kumagai, H.; Kitagawa, S.; Honda, K.; Enomoto, M.; Katada, M. *Mol. Cryst. Liq. Cryst.* **1996**, *286*, 51.
(22) Kondo, M.; Yoshitomi, T.; Seki, K.; Matsuzaka, H.; Kitagawa, S. *Angew. Chem., Int. Ed. Engl.* **1997**, *36*, 1725.
(23) Baxter, P. N. W.; Lehn, J.-M.; Kneisel, B. O.; Fenske, D. *Angew. Chem., Int. Ed. Engl.* **1997**, *36*, 1978.
(24) Schauer, C. L.; Matwey, E.; Fowler, F. W.; Lauher, J. W. *J. Am. Chem. Soc.* **1997**, *119*, 10245.
(25) Dai, J.; Yamamoto, M.; Kuroda-Sowa, T.; Maekawa, M.; Suenaga, Y.; Munakata, M. *Inorg. Chem.* **1997**, *36*, 2688.
(26) Yaghi, O. M.; Li, G. *Angew. Chem., Int. Ed. Engl.* **1995**, *34*, 207.
(27) Fujita, M.; Kwon, Y. J.; Washizu, S.; Ogura, K. *J. Am. Chem. Soc.* **1994**, *116*, 1151.
(28) Whiteside, G. M.; Simanek, E. E.; Mathias, J. P.; Seto, C. T.; Chin, D. N.; Mammen, M.; Gordon, D. M. *Acc. Chem. Res.* **1995**, *28*, 37.
(29) Scudder, M.; Dance, I. *J. Chem. Soc., Dalton Trans.* **1998**, 329.
(30) Oliver, S.; Kuperman, A.; Ozin, G. A. *Angew. Chem., Int. Ed. Engl.* **1998**, *37*, 47.
(31) Kawata, S.; Breeze, S. R.; Wang, S.; Greedan, J. E.; Raju, N. P. *J. Chem. Soc., Dalton Trans.* **1997**, 717.
(32) Endo, K.; Ezuhara, T.; Koyanagi, M.; Masuda, H.; Aoyama, Y. *J. Am. Chem. Soc.* **1997**, *119*, 499.
(33) Carlucci, L.; Ciani, G.; Proserpio, D. M.; Sironi, A. *J. Chem. Soc., Dalton Trans.* **1997**, 1801.
(34) Yaghi, O. M.; Li, H.; Groy, T. L. *J. Am. Chem. Soc.* **1996**, *118*, 9096.
(35) Ouahab, L. *Chem. Mater.* **1997**, *9*, 1909.
(36) Ballester, L.; Gutiérrez, A.; Perpiñán, M. F.; Amador, U.; Azcondo, M. T.; Sánchez, A. E.; Bellitto, C. *Inorg. Chem.* **1997**, *36*, 6390.
(37) Kaim, W.; Moscherosch, M. *Coord. Chem. Rev.* **1994**, *129*, 157.
(38) Kuroda-Sowa, T.; Horino, T.; Yamamoto, M.; Ohno, Y.; Maekawa, M.; Munakata, M. *Inorg. Chem.* **1997**, *36*, 6382.
(39) Dei, A.; Gatteschi, D.; Pardi, L.; Russo, U. *Inorg. Chem.* **1991**, *30*, 2589.
(40) Liu, S.; Shaikh, S. N.; Zubieta, J. *Inorg. Chem.* **1989**, *28*, 723.
(41) Wrobleski, J. T.; Brown, D. B. *Inorg. Chem.* **1979**, *18*, 498.
(42) Wrobleski, J. T.; Brown, D. B. *Inorg. Chem.* **1979**, *18*, 2738.

Table 1. Crystallographic Data for $\{[M(CA)(H_2O)_2](H_2O)\}_n$

compd	$\{[Fe(CA)(H_2O)_2](H_2O)\}_n$ (**1a**)	$\{[Co(CA)(H_2O)_2](H_2O)\}_n$ (**1b**)	$\{[Mn(CA)(H_2O)_2](H_2O)\}_n$ (**1c**)
formula	$FeC_6O_7Cl_2H_6$	$CoC_6O_7Cl_2H_6$	$MnC_6O_7Cl_2H_6$
fw	316.86	319.95	315.95
dimens (mm^3)	0.15 × 0.10 × 0.05	0.10 × 0.10 × 0.05	0.20 × 0.20 × 0.05
space group	*C*2/*c* (No. 15)	*C*2/*c* (No. 15)	*C*2/*c* (No. 15)
cryst syst	monoclinic	monoclinic	monoclinic
a (Å)	4.914(2)	4.927(4)	4.904(2)
b (Å)	14.222(2)	14.067(4)	14.288(2)
c (Å)	13.987(2)	14.007(3)	14.080(1)
β (deg)	94.98(2)	96.05(4)	94.11(2)
V ($Å^3$)	973.8(4)	965.4(8)	984.1(3)
Z	4	4	4
D_{calcd} (g/cm^3)	2.161	2.201	2.132
F(000)	632.00	636.00	628.00
μ(Mo Kα) (cm^{-1})	21.11	23.48	18.99
diffractometer	AFC7R	AFC7R	AFC7R
temp (°C)	23.0	23.0	23.0
$2\theta_{max}$ (deg)	55.1	55.0	55.1
reflns collcd	1316	1303	1331
unique reflcns	1179	1168	1193
no. of obsd reflcns	719 ($I > 3\sigma$)	876 ($I > 2\sigma$)	853 ($I > 3\sigma$)
no. of variables	87	87	86
R^a	0.045	0.029	0.028
$R_w{}^b$	0.045	0.027	0.025
GOF	1.28	1.28	1.50

[a] $R = \sum||F_o| - |F_c||/\sum|F_o|$. [b] $R_w = [(\sum w(|F_o| - |F_c|)^2/\sum wF_o^2)]^{1/2}$, $w = 4F_o^2/\sigma^2(F_o^2)$.

similar to that employed for **1a**. Red-purple plate crystals began to form in a week for **1b**. Anal. Calcd for $CoCl_2O_7C_6H_6$: C, 23.86; H, 1.33. Found: C, 22.56; H, 1.82. Red-purple plate crystals began to form in a week for **1c**. Anal. Calcd for $MnCl_2O_7C_6H_6$: C, 22.81; H, 1.91. Found: C, 22.94; H, 1.88.

Syntheses of $\{[M(CA)(H_2O)_2](phz)\}_n$ (2a−c). *2a*. An aqueous solution (10 mL) of iron(II) sulfate heptahydrate (6 × 10^{-5} mol) was transferred to a glass tube, and then an ethanol−water (1:1) mixture (10 mL) of phenazine (phz) (6 × 10^{-5} mol) and H_2CA (6 × 10^{-5} mol) was poured into the tube without mixing the two solutions under nitrogen atmosphere. Dark green plate crystals began to form in one week. One of these crystals was used for X-ray crystallography. Physical measurements were conducted on a polycrystalline powder that was synthesized as follows: An aqueous solution (100 mL) of H_2CA (6 × 10^{-4} mol) was added to a 6 × 10^{-4} mol amount of iron(II) sulfate heptahydrate and a 6 × 10^{-4} mol amount of phenazine dissolved in an ethanol−water (1:1) mixture (20 mL) under a nitrogen atmosphere. Upon stirring of the mixture, the dark green powder appeared immediately. Anal. Calcd for $FeCl_2O_6N_2C_{18}H_{12}$: C, 45.13; H, 2.52; N, 5.85. Found: C, 44.98; H, 2.56; N, 5.86. IR (KBr pellet): 3283 s, 3077 s, 1676 w, 1619 w, 1522 vs, 1510 vs, 1437 w, 1375 m, 1292 w, 1217 w, 1150 w, 1125 w, 1002 w, 978 w, 849 s, 758 s, 700 w, 603 w, 592 w, 577 w cm^{-1}. The identity of the magnetic and X-ray batches has been confirmed by their XRD patterns.

$\{[M(CA)(H_2O)_2](phz)\}_n$ (M = Co^{2+} (**2b**), Mn^{2+} (**2c**)) were synthesized from cobalt(II) sulfate heptahydrate and manganese(II) chloride tetrahydrate, respectively, by a procedure similar to that employed for **2a**. Red-purple plate crystals began to form in 1 week for **2b**. Anal. Calcd for $CoCl_2O_6N_2C_{18}H_{12}$: C, 44.84; H, 2.51; N, 5.81. Found: C, 44.68; H, 2.56; N, 5.84. Red-purple plate crystals began to form in a week for **2c**. Anal. Calcd for $MnCl_2O_6N_2C_{18}H_{12}$: C, 45.22; H, 2.52; N, 5.86. Found: C, 45.06; H, 2.44; N, 5.91.

Physical Measurements. The IR spectra of the KBr disks were measured on a Hitachi I-5040 FT-IR spectrophotometer. UV and visible spectra were measured on a Hitachi U-3500 spectrophotometer. EPR spectra were recorded at X-band frequency with a JEOL RE−3X spectrometer operating at 9.1−9.5 GHz. The resonance frequency was measured on an Anritsu MF76A microwave frequency counter. The magnetic fields were calibrated by an Echo Electronics EFM-2000AX NMR field meter. The EPR spectra were measured with modulation frequency of 100 kHz and modulation amplitude of 0.5 mT, throughout. The ^{57}Fe Mössbauer spectra were obtained by using an Wissel Mössbauer spectrometer with a proportional counter. A ^{57}Co(Rh) source moving in a constant-acceleration mode was used for the measurements. The velocity scale was calibrated by using a metallic iron-foil spectrum. The isomer shift (IS) and the quadrupole splitting (QS) were obtained by least-squares fitting of the Mössbauer data to Lorentzian line shapes. Magnetic susceptibility data were recorded over the temperature range from 2 to 300 K at 1 T with a SQUID susceptometer (Quantum Design, San Diego, CA) interfaced with an HP Vectra computer system. All data were corrected for diamagnetism which was calculated from Pascal's table. X-ray powder diffraction data were collected on a MAC Science MXP18 automated diffractometer by using Cu Kα radiation. Thermal gravimetric (TG) analysis and differential scanning calorimetry (DSC) were carried out with a Seiko Instruments SSC5200 thermo-analyzer in nitrogen atmosphere (heating rates: 10 K/min for TG; 2−5 K/min for DSC).

Crystallographic Data Collection and Refinement of the Structure. A suitable crystal was chosen and mounted on a glass fiber with epoxy resin. Data collections were carried out on a Rigaku AFC7R with graphite-monochromated Mo Kα radiation (λ = 0.710 69 Å). Cell constants and the orientation matrix for intensity data collection for each crystal were based on the setting angles of 23−25 carefully centered reflections in the ranges 20.68° < 2θ < 23.90°, 20.60° < 2θ < 24.02°, and 20.73° < 2θ < 36.59°, for **1a**−**1c**, respectively, and 26.49° < 2θ < 35.48°, 20.30° < 2θ < 24.14°, and 20.26° < 2θ < 24.98°, for **2a**−**c**, respectively. Crystallographic data are given in Tables 1 and 2. The structures were solved by direct methods (Rigaku TEXSAN crystallographic software package of Molecular Structure Corp.). Full-matrix least-squares refinements were carried out with anisotropic thermal parameters for all non-hydrogen atoms. All the hydrogen atoms were located in the Fourier difference maps. Hydrogen atoms were refined isotropically for **1a**−**c** whereas, for **2a**−**c**, hydrogen atoms were not refined. Atomic coordinates are given in Table 3.

Results and Discussion

Crystal Structure of 1a−c. All the compounds, **1a**−**c**, are isostructural with one-dimensional "type I" chains. An ORTEP drawing of **1a** is shown in Figure 1a. The selected bond distances and angles with their estimated standard deviations for **1a**−**c** are listed in

Table 2. Cyrstallographic Data for $\{[M(CA)(H_2O)_2](phz)\}_n$

compd	$\{[Fe(CA)(H_2O)_2](phz)\}_n$ (**2a**)	$\{[Co(CA)(H_2O)_2](phz)\}_n$ (**2b**)	$\{[Mn(CA)(H_2O)_2](phz)\}_n$ (**2c**)
formula	$FeC_{18}O_6Cl_2N_2H_{12}$	$CoC_{18}O_6Cl_2N_2H_{12}$	$MnC_{18}O_6Cl_2N_2H_{12}$
fw	479.06	482.14	478.15
dimens (mm^3)	0.50 × 0.20 × 0.05	0.20 × 0.20 × 0.05	0.15 × 0.15 × 0.05
space group	$P\bar{1}$ (No. 2)	$P\bar{1}$ (No. 2)	$P\bar{1}$ (No. 2)
cryst syst	triclinic	triclinic	triclinic
a (Å)	8.079(2)	7.959(2)	8.178(1)
b (Å)	11.366(3)	11.362(3)	11.433(1)
c (Å)	5.055(2)	5.074(2)	5.0684(5)
α (deg)	96.57(3)	96.69(3)	96.121(9)
β (deg)	98.70(3)	98.29(2)	98.477(9)
γ (deg)	83.07(2)	83.21(2)	83.398(10)
V ($Å^3$)	453.3(3)	448.5(2)	463.68(9)
Z	1	1	1
D_{calcd} (g/cm^3)	1.755	1.785	1.712
$F(000)$	242.00	243.00	241.00
μ(Mo Kα) (cm^{-1})	11.67	12.96	10.40
diffractometer	AFC7R	AFC7R	AFC7R
temp (°C)	23.0	23.0	23.0
$2\theta_{max}$ (deg)	55.1	55.1	55.1
reflns collcd	2250	2229	2307
unique reflcns	2100	2078	2156
no. of obsd reflcns ($I > 3\sigma$)	1560	1361	1345
no. of variables	134	133	133
R^a	0.031	0.035	0.032
$R_w{}^b$	0.023	0.031	0.030
GOF	2.29	1.66	1.33

[a] $R = \sum||F_o| - |F_c||/\sum|F_o|$. [b] $R_w = [(\sum w(|F_o| - |F_c|)^2/\sum wF_o^2)]^{1/2}$, $w = 4F_o^2/\sigma^2(F_o^2)$.

Table 4. The atom labeling scheme for **1b**,**c** is the same as that for **1a**. Each metal atom has a distorted cis-octahedral coordination geometry. The two water molecules in the cis position and four oxygen atoms of two CA^{2-} dianions create an octahedral environment around the metal ion. There are three pairs of different M−O distances, for example, 2.123(4) Å (Fe−O(1) and Fe−O(1′)), 2.153(4) Å (Fe−O(2), Fe−O(2′)), and 2.083(5) Å (Fe−O(3), Fe−O(3′)). The mean M−O distance of **1c** (2.19 Å) is longer than that in **1a** (2.12 Å) and **1b** (2.09 Å), because of the larger ionic radius of the manganese(II) ion. The asymmetrical coordination of the CA^{2-} dianion in **1c** is recognized from the two C−O bond distances (C(1)−O(1), 1.252(3) Å, C(2)−O(2), 1.262(3) Å). However, the two C−O distances in **1a**,**1b** are similar (C(1)−O(1), 1.255(6) Å (**1a**), 1.258(3) Å (**1b**); C(2)−O(2), 1.259(6) Å (**1a**), 1.257(3) Å (**1b**)). The type I zigzag chain runs along the diagonal between the *a* and *c* axes (Figure 1b). The metal−metal distances in the chains are 8.077(2) Å (**1a**), 7.992(1) Å (**1b**), and 8.201(1) Å (**1c**). This order of the distances is in accordance with those for the ionic radii and the bond distances around the metals. The chain structure of **1a**−**c** is close to those of $[Zn((NO_2)_2\text{-DHBQ})_2(H_2O)_2]_n$[43] and $[M(Et_2\text{-DHBQ})_2(H_2O)_3]_n$ (M = Ca^{2+}, Sr^{2+}, and Ba^{2+})[44,45] but different from those of $[Cu(CA)(H_2O)_2]_k$[6,46] and **2a**−**c** (vide infra). The choice of the metal element is related to the chain type; namely, the chain structure can be delicately tuned.

There are interstitial water molecules which are hydrogen bonded to the nearest-neighbor coordinated waters and oxygen atoms on the CA^{2-}. The zigzag chains are linked by three types of hydrogen bonds shown in Figure 1c, giving a sandwich structure. The first type of hydrogen bonding (O(3)−O(1″); 2.885(6) Å (**1a**), 2.870(4) Å (**1b**), and 2.866(3) Å (**1c**)) occurs between the coordinated waters and the oxygen atoms on the adjacent CA^{2-} anion in the nearest-neighbor chain and links the chains to form a 2D sheet spreading out along the *ac* plane. A similar connectivity has been found in $[Ca(Et_2\text{-DHBQ})_2(H_2O)_3]_n$,[45] where the hydrogen bonding distance (3.094(7) Å) is longer than those in **1a**−**c**. The sheet structure differs from the notched sheet structure of $\{[Cu(CA)(H_2O)_2](H_2O)\}_n$.[46] This is due to the coordination geometry of the water molecules on the metal, where the water molecules sit on trans positions. The second type of hydrogen bonding occurs between the uncoordinated water and the oxygen atom on the adjacent CA^{2-} anion in the nearest-neighbor chain (O(4)−O(2); 2.800(5) Å (**1a**), 2.735(4) Å (**1b**), and 2.822(3) Å (**1c**)), resulting in a linkage of the nearest-neighbor chains in the sheet, $\{[M(CA)(H_2O)_2]_k\}_l$. These hydrogen bond distances decrease with decreasing ionic radii, and this tendency is in accordance with the O(1)−M−O(2′) angle (105.0(1)° (**1a**), 104.5(1)° (**1b**), and 105.4(1)° (**1c**)), suggesting that fine-tuning of the hydrogen−bonding interaction is associated with the chosen metal ion. The third type of hydrogen bonding occurs between the coordinated waters and the uncoordinated water (O(3″)−O(4); 2.751(7) Å (**1a**), 2.744(4) Å (**1b**), and 2.735(4) Å (**1c**)). The interstitial water molecules interlink the nearest-neighbor sheets, $\{[M(CA)(H_2O)_2]_k\}_l$, resulting in novel intercalation compounds.

Crystal Structure of 2a−c. X-ray crystallography also reveals that **2a**−**c** are isostructural with one-dimensional "type II" chains. An ORTEP drawing of **2a** is shown in Figure 2a, where the metal atom sits on the crystallographic inversion center. The selected bond distances and angles with their estimated standard deviations for **2a**−**c** are listed in Table 5. The atom-labeling scheme for **2b**,**2c** is the same as that for **2a**. The geometry around the metal ion is a distorted

(43) Robl, C.; Weiss, A. *Z. Naturforsch.* **1986**, *41b*, 1337.
(44) Robl, C. *Mater. Res. Bull.* **1987**, *22*, 1395.
(45) Robl, C.; Kuhs, W. F. *J. Solid State Chem.* **1989**, *79*, 46.
(46) Kawata, S.; Kitagawa, S.; Kondo, M.; Katada, M. *Synth. Met.* **1995**, *71*, 1917.

Table 3. Positional and Equivalent Isotropic Thermal Parameters

atom	*x*	*y*	*z*	*B*(eq)[a](Å)
		(a) **1a**		
Fe	1.5000	0.12189(9)	0.7500	1.61(3)
Cl	1.2807(3)	0.4025(1)	0.9630(1)	2.06(3)
O(1)	1.8169(8)	0.1216(3)	0.8633(3)	1.87(8)
O(2)	1.3986(8)	0.2348(3)	0.8430(3)	1.78(9)
O(3)	1.287(1)	0.0162(3)	0.8150(4)	2.5(1)
O(4)	1.0000	0.3515(5)	0.7500	3.0(2)
C(1)	1.794(1)	0.1780(4)	0.9312(4)	1.6(1)
C(2)	1.559(1)	0.2478(4)	0.9169(4)	1.5(1)
C(3)	1.537(1)	0.3196(4)	0.9832(4)	1.5(1)
		(b) **1b**		
Co	0.5000	0.12487(4)	0.7500	1.60(1)
Cl	0.2778(2)	0.40293(6)	0.96314(5)	2.16(2)
O(1)	0.8181(4)	0.1233(2)	0.8618(1)	1.94(4)
O(2)	0.3978(4)	0.2367(2)	0.8409(1)	1.85(4)
O(3)	0.2934(6)	0.0214(2)	0.8173(2)	2.58(6)
O(4)	1.0000	0.3562(3)	0.7500	3.32(9)
C(1)	0.7940(6)	0.1786(2)	0.9310(2)	1.57(6)
C(2)	0.5584(5)	0.2489(2)	0.9158(2)	1.51(6)
C(3)	0.5363(6)	0.3200(2)	0.9832(2)	1.61(6)
		(c) **1c**		
Mn	0.0000	0.11833(4)	0.2500	1.60(1)
Cl	−0.2172(1)	0.40173(5)	0.46184(5)	1.95(2)
O(1)	0.3220(4)	0.1205(1)	0.3662(1)	1.86(4)
O(2)	−0.0967(4)	0.2340(1)	0.3443(1)	1.69(4)
O(3)	−0.2203(5)	0.0109(2)	0.3162(2)	2.73(6)
O(4)	−0.5000	0.3483(2)	0.2500	2.86(8)
C(1)	0.2956(5)	0.1771(2)	0.4328(2)	1.43(6)
C(2)	0.0621(5)	0.2474(2)	0.4176(2)	1.36(6)
C(3)	0.0387(5)	0.3196(2)	0.4824(2)	1.34(5)
		(d) **2a**		
Fe	1.0000	0.0000	1.0000	1.67(1)
Cl	1.42703(9)	0.19283(6)	0.5792(1)	2.25(2)
O(1)	1.2407(2)	−0.0820(2)	1.1676(4)	1.97(4)
O(2)	1.1774(2)	0.0796(2)	0.8238(4)	1.79(4)
O(3)	1.0136(2)	0.1298(2)	1.3254(4)	2.51(5)
N	1.0035(3)	0.3774(2)	0.4114(5)	2.44(6)
C(1)	1.3668(3)	−0.0473(2)	1.0971(5)	1.51(6)
C(2)	1.3322(3)	0.0462(2)	0.8972(5)	1.46(6)
C(3)	1.4658(3)	0.0885(2)	0.8105(5)	1.55(6)
C(4)	0.7142(4)	0.4067(3)	0.8987(7)	3.23(8)
C(5)	0.8075(4)	0.3576(3)	0.7085(7)	2.95(8)
C(6)	0.9065(4)	0.4280(2)	0.5940(6)	2.35(7)
C(7)	1.0971(4)	0.4471(3)	0.3142(6)	2.36(7)
C(8)	1.1991(4)	0.3982(3)	0.1163(7)	2.78(7)
C(9)	1.2892(4)	0.4696(3)	0.0097(7)	3.17(8)
		(e) **2b**		
Co	0.5000	0.5000	0.0000	1.64(2)
Cl	0.0727(9)	0.30796(9)	0.4203(2)	2.22(2)
O(1)	0.2634(3)	0.5814(2)	−0.1696(5)	1.91(6)
O(2)	0.3262(3)	0.4202(2)	0.1729(5)	1.79(6)
O(3)	0.4904(3)	0.3712(2)	−0.3224(5)	2.27(6)
N	0.4960(4)	0.1228(3)	0.5869(7)	2.49(8)
C(1)	0.1352(4)	0.5473(3)	−0.0977(7)	1.40(8)
C(2)	0.1704(4)	0.4533(3)	0.1034(7)	1.48(8)
C(3)	0.0338(4)	0.4119(3)	0.1886(7)	1.47(8)
C(4)	0.7863(5)	0.0935(4)	0.0926(9)	3.1(1)
C(5)	0.6924(5)	0.1433(4)	0.2854(9)	2.9(1)
C(6)	0.5939(5)	0.0720(3)	0.4023(8)	2.30(9)
C(7)	0.4017(5)	0.0528(3)	0.6864(8)	2.41(9)
C(8)	0.2995(5)	0.1006(4)	0.8882(9)	2.9(1)
C(9)	0.2103(5)	0.0288(4)	0.9980(9)	3.1(1)
		(f) **2c**		
Mn	0.0000	0.5000	0.0000	1.88(2)
Cl	0.43003(9)	0.69297(7)	−0.4200(2)	2.46(2)
O(1)	0.2432(2)	0.4173(2)	0.1689(4)	2.24(5)
O(2)	0.1836(2)	0.5797(2)	−0.1762(4)	2.07(5)
O(3)	0.0158(3)	0.6320(2)	0.3322(4)	2.73(5)
N	0.0004(3)	0.8786(2)	−0.5863(5)	2.79(6)
C(1)	0.3682(3)	0.4526(2)	0.0985(6)	1.64(6)
C(2)	0.3346(3)	0.5467(2)	−0.1024(5)	1.60(6)
C(3)	0.4675(3)	0.5885(2)	−0.1886(6)	1.72(6)
C(4)	−0.2862(4)	0.9103(3)	−0.1012(8)	3.74(9)
C(5)	−0.1953(4)	0.8603(3)	−0.2905(7)	3.42(9)
C(6)	−0.0952(4)	0.9294(3)	−0.4038(7)	2.72(8)
C(7)	0.0956(4)	0.9471(3)	−0.6832(7)	2.70(8)
C(8)	0.1964(4)	0.8984(3)	−0.8819(7)	3.39(9)
C(9)	0.2880(4)	0.9678(3)	−0.9850(7)	3.72(9)

[a] $B(\text{eq}) = {}^8/_3\pi^2(U_{11}(aa^*)^2 + U_{22}(bb^*)^2 + U_{33}(cc^*)^2 + 2U_{12}aa^*bb^* \cos\gamma + 2U_{13}aa^*cc^* \cos\beta + 2U_{23}bb^*cc^* \cos\alpha)$.

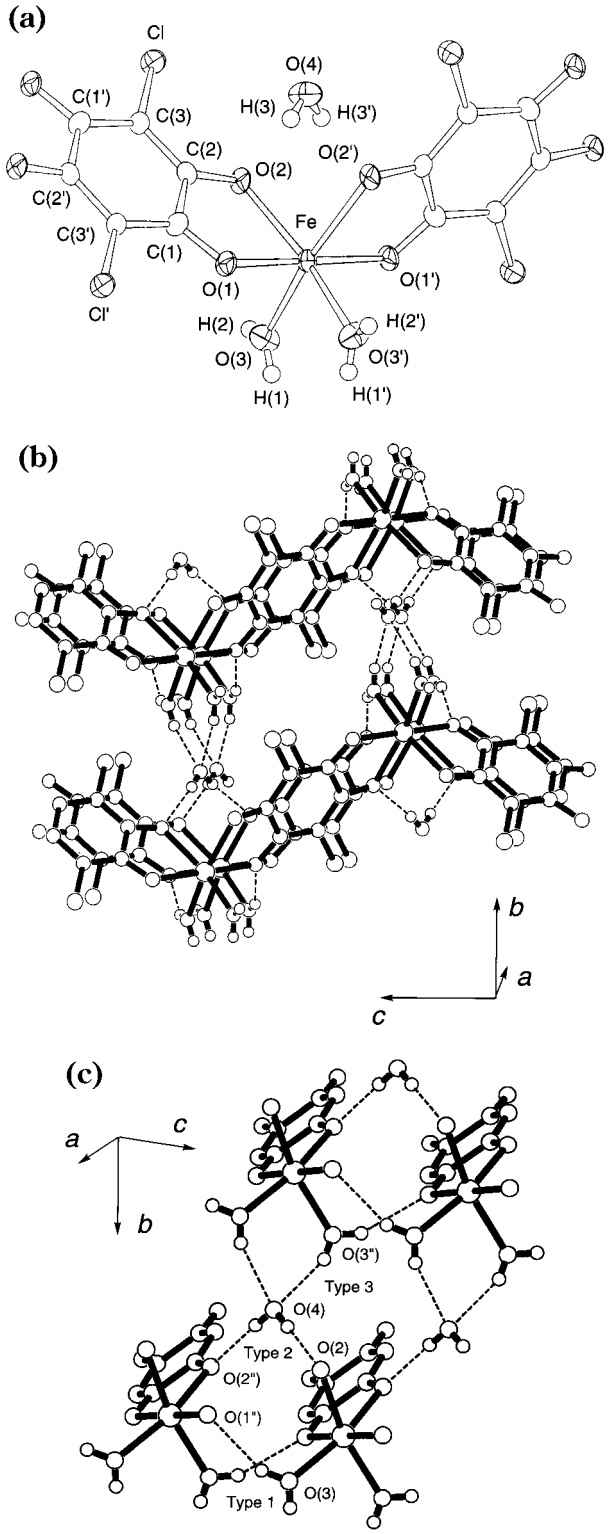

Figure 1. (a) ORTEP drawing of a monomer unit of compound **1a** with labeling scheme and thermal ellipsoids at the 50% probability level for Fe, Cl, O, and C atoms. Spheres of the hydrogen atoms have been arbitrarily reduced. Projection of **1a** perpendicular to the chain (b) and along the chain (c). The dashed lines denote the sites of hydrogen bonding between the molecules.

octahedron involving the four oxygen atoms of two CA^{2-} anions and two water molecules, which sit on trans positions relative to each other. It is interesting to note that the coordination geometry and bond lengths around the iron in **2a** is similar to those of $[Fe(C_2O_4)(H_2O)_2]_n$[47]

Table 4. Bond Distances (Å) and Angles (deg) for $\{[M(CA)(H_2O)_2](H_2O)\}_n$

Distances

	1a	1b	1c
M−O(1)	2.123(4)	2.096(2)	2.192(2)
M−O(2)	2.153(4)	2.117(2)	2.194(2)
M−O(3)	2.083(5)	2.060(3)	2.130(3)
O(1)−C(1)	1.255(6)	1.258(3)	1.252(3)
O(2)−C(2)	1.259(6)	1.257(3)	1.262(3)
C(1)−C(2)	1.523(7)	1.523(4)	1.527(4)
C(2)−C(3)	1.389(7)	1.387(4)	1.387(3)
C(3)−C(1)	1.400(3)	1.390(4)	1.395(3)
C(3)−Cl	1.731(6)	1.728(3)	1.728(3)
M−M′	4.914(2)	4.927(4)	4.904(2)
M−M″	7.523(8)	7.452(1)	7.553(1)
M−M‴	8.077(2)	7.992(1)	8.201(1)

Angles

	1a	1b	1c
O(1)−M−O(2)	75.1(1)	76.41(8)	73.31(7)
O(1)−M−O(3)	92.0(2)	91.0(1)	92.55(9)
O(1)−M−O(1′)	179.8(2)	178.8(1)	178.4(1)
O(1)−M−O(2′)	105.0(1)	104.52(8)	105.43(7)
O(1)−M−O(3′)	87.8(2)	88.2(1)	88.62(9)
O(2)−M−O(3)	97.1(2)	95.12(9)	98.03(9)
O(2)−M−O(2′)	83.5(2)	84.1(1)	82.2(1)
O(2)−M−O(3′)	162.4(2)	163.75(9)	161.18(8)
O(3)−M−O(3′)	87.7(3)	90.1(2)	87.8(2)
M−O(1)−C(1)	117.1(2)	116.4(2)	117.4(2)
M−O(2)−C(2)	116.8(2)	115.8(2)	117.5(2)
C(2)−C(1)−C(3′)	119.1(2)	119.4(3)	118.8(2)
C(1)−C(2)−C(3)	119.7(5)	119.1(2)	119.6(2)
C(2)−C(3)−C(1′)	121.0(5)	121.1(3)	121.1(2)

Hydrogen Bond Distances

	1a	1b	1c
O(1″)−O(3)	2.885(6)	2.870(3)	2.866(3)
O(2)−O(4)	2.800(5)	2.787(3)	2.822(3)
O(3″)−O(4)	2.751(7)	2.744(4)	2.753(4)

and different from those of **1a**. There are three pairs of different M−O distances, for example, 2.148(2) Å (Fe−O(1) and Fe−O(1′)), 2.133(2) Å (Fe−O(2), Fe−O(2′)), and and 2.079(2) Å (Fe−O(3), Fe−O(3′)). The mean M−O distance of **2c** (2.17 Å) is longer than those of **2a** (2.12 Å) and **2b** (2.09 Å), because of the larger ionic radius of the manganese(II) ion as found in **1a**−**c**. The asymmetrical coordination of the CA^{2-} dianion is recognized in the different distances of the C−O bonds; the distance of C(1)−O(1) (1.249(3) Å (**2a**), 1.248(4) Å (**2b**), and 1.253(3) Å (**2c**)) is similar to those reported for the free chloranilate dianion (1.243(7), 1.253(7) Å),[48] and another distance of C(2)−O(2) (1.274(3) Å (**2a**), 1.264(4) Å (**2b**), and 1.262(3) Å (**2c**)) is close to that of a *p*-quinone form found in $[Cu(CA)(pz)]_n$ and $\{[Cu(CA)(H_2O)](H_2O)\}_n$.[46,49] This feature is different from that of **1a**−**c** and similar to that of $\{[Cu(CA)(H_2O)_2](phz)\}_n$.[6]

The crystal packing structure consists of uncoordinated phz molecules and one-dimensional $[M(CA)(H_2O)_2]_k$ chains, both of which form a layer structure (Figure 2b,c). The type II straight chain runs along the *a* axis, whereas **1a**−**c** consists of zigzag chains (type I). The coplanarity of the CA^{2-} and MO_4 planes in the chain of **2a**−**c** (**2a** (178.5°), **2b** (178.7°), and **2c** (178.8°)) is realized, as seen in $\{[Cu(CA)(H_2O)_2](phz)\}_n$ (179.9°).[6]

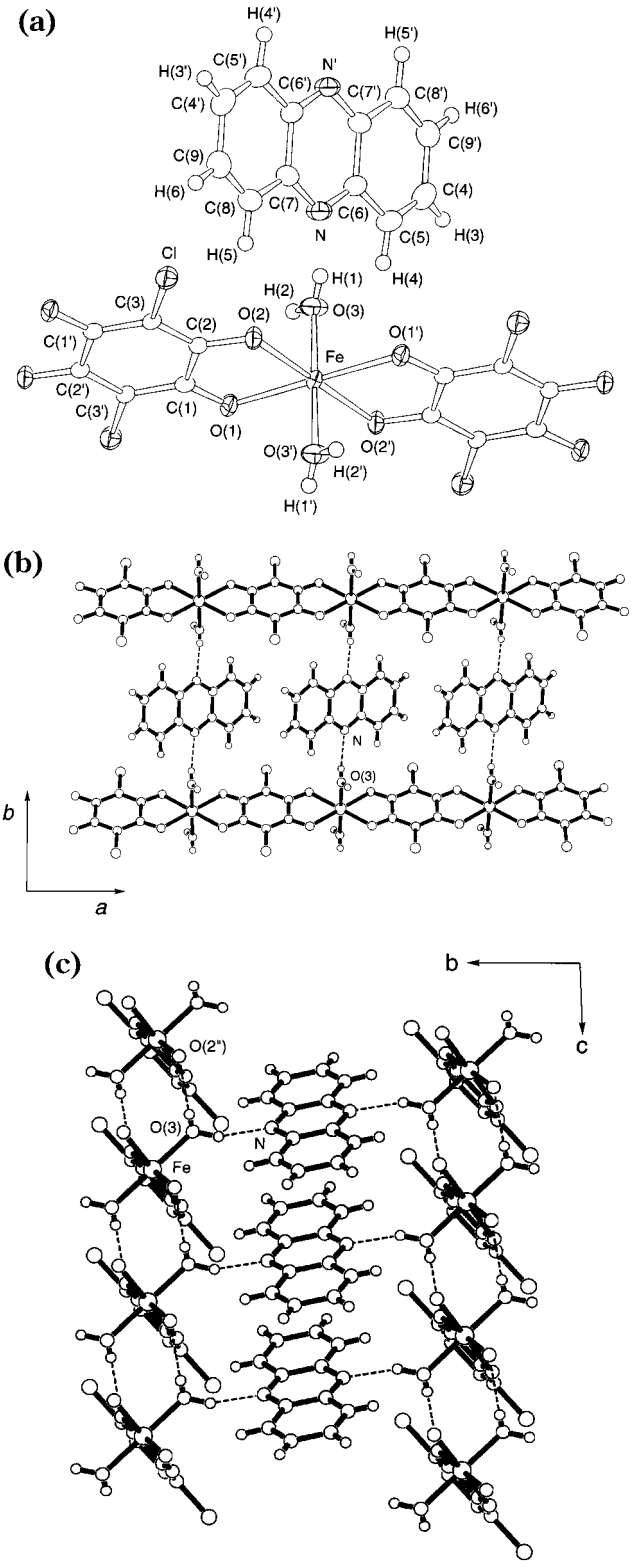

Figure 2. (a) ORTEP drawing of a monomer unit of compound **2a** with labeling scheme and thermal ellipsoids at the 50% probability level for Fe, Cl, O, N, and C atoms. Spheres of the hydrogen atoms have been arbitrarily reduced. Projection of **2a** along the *c* axis (b) and the *a* axis (c). The dashed lines denote the sites of hydrogen bonding between the molecules.

The features of the chain structures for **2a**−**c** are very close to those of $\{[Cu(CA)(H_2O)_2](phz)\}_n$, despite the differences between the nature of the metals. The metal−metal distances in the chains are 8.079(1) Å (**2a**), 7.960(2) Å (**2b**), and 8.178(1) Å (**2c**), respectively. This

(47) Mazzi, C.; Caravelli, F. *Period. Mineral.* **1957**, *26*, 2.
(48) Andersen, E. K. *Acta Crystallogr.* **1967**, *22*, 191.
(49) Kawata, S.; Kitagawa, S.; Kondo, M.; Furuchi, I.; Munakata, M. *Angew. Chem., Int. Ed. Engl.* **1994**, *33*, 1759.

Table 5. Bond Distances (Å) and Angles (deg) for {[M(CA)(H$_2$O)$_2$](phz)}$_n$

Distances

	2a	2b	2c
M−O(1)	2.148(2)	2.109(2)	2.196(2)
M−O(2)	2.133(2)	2.083(2)	2.184(2)
M−O(3)	2.079(2)	2.063(2)	2.137(2)
O(1)−C(1)	1.249(3)	1.248(4)	1.253(3)
O(2)−C(2)	1.274(3)	1.264(4)	1.262(3)
C(1)−C(2)	1.523(4)	1.537(5)	1.534(4)
C(2)−C(3)	1.380(3)	1.377(5)	1.380(4)
C(3)−C(1)	1.404(4)	1.400(5)	1.398(4)
C(3)−Cl	1.729(3)	1.733(3)	1.733(3)
C(4)−C(5)	1.341(4)	1.355(6)	1.340(5)
C(5)−C(6)	1.419(4)	1.418(6)	1.418(4)
N−C(6)	1.336(4)	1.339(5)	1.341(4)
N−C(7)	1.337(4)	1.340(5)	1.340(4)
C(6)−C(7)	1.441(4)	1.435(5)	1.433(4)
C(7)−C(8)	1.414(4)	1.421(5)	1.422(4)
C(8)−C(9)	1.357(4)	1.348(6)	1.344(4)
C(4)−C(9′)	1.428(4)	1.411(6)	1.414(5)
M−M′	5.055(2)	5.074(2)	5.068(1)
M−M″	8.079(2)	7.959(2)	8.178(1)
M−M‴	11.366(3)	11.362(3)	11.433(1)

Angles

	2a	2b	2c
O(1)−M−O(2)	75.65(7)	77.59(9)	74.21(7)
O(1)−M−O(3)	88.71(8)	88.8(1)	88.48(8)
O(2)−M−O(3)	90.89(7)	91.3(1)	90.43(8)
M−O(1)−C(1)	116.3(2)	115.2(2)	116.6(2)
M−O(2)−C(2)	116.2(2)	115.8(2)	116.9(2)
C(2)−C(1)−C(3′)	119.2(2)	119.3(3)	119.1(2)
C(1)−C(2)−C(3)	119.3(2)	118.6(3)	119.0(2)
C(1′)−C(3)−C(2)	121.5(2)	122.1(3)	121.9(2)
C(5)−C(4)−C(9′)	121.3(3)	121.6(4)	121.4(3)
C(4)−C(5)−C(6)	120.5(3)	119.9(4)	119.9(3)
C(5)−C(6)−C(7′)	118.3(3)	118.9(4)	119.1(3)
N−C(6)−C(7′)	121.7(3)	121.5(4)	121.0(3)
C(6)−N−C(7)	117.6(3)	117.6(3)	117.7(3)
N−C(7)−C(6′)	120.7(3)	120.9(4)	121.4(3)
C(6′)−C(7)−C(8)	119.6(3)	118.8(4)	118.6(3)
C(7)−C(8)−C(9)	119.8(3)	120.4(4)	120.1(3)
C(8)−C(9)−C(4′)	120.5(3)	120.5(4)	120.9(3)

Hydrogen Bond Distances

	2a	2b	2c
O(2″)−O(3)	2.750(3)	2.787(3)	2.751(2)
N−O(3)	2.791(3)	2.803(4)	2.796(3)

order of the distances is also in accordance with those of the ionic radii and bond distances around the metals as seen in the type I chains in **1a**−**c**. Interestingly, the straight chains of **2a**−**c** are linked by two types of hydrogen bonds. The first type of hydrogen bonding (O(3)−O(2″); 2.750(3) Å for **2a**) occurs between the coordinated waters and the oxygen atoms on the adjacent CA^{2-} anion and links the chains to form a 2-D sheet, {[M(CA)(H$_2$O)$_2$]$_k$}$_l$, spreading out along the *ac* plane. This hydrogen bonding distance of **2a** is shorter than that of **2b** (2.787(3) Å) but is the same order of magnitude for that of **2c** (2.751(2) Å). Such a relationship is not found in **1a**−**c**. Moreover, the modes of the hydrogen bonds in the sheet of **2a**−**c** and the sheet structures are similar to those of {[Cu(CA)(H$_2$O)$_2$](phz)}$_n$, which is isomorphous to **2a**−**c**, but differs from those of **1a**−**c**. This is due to the variety of the hydrogen-bonding capability of the interstitial water molecules between the sheets and the existence of additional hydrogen-bonding possibilities. Thus the intercalated guest molecules affect the sheet structure of {[M(CA)(H$_2$O)$_2$]$_k$}$_l$ as well as the chain structure. The second type of the hydrogen bonding occurs between the uncoordinated phz and the coordinated water (N−O(3); 2.791(3) Å (**2a**), 2.803(4) Å (**2b**), and 2.796(3) Å (**2c**)). {[M(CA)(H$_2$O)$_2$](phz)}$_n$ sheets sandwich the phz molecules, which serve as not a linking ligand but a hydrogen acceptor. This hydrogen bond interlinks the nearest-neighbor sheets, resulting in an intercalation compound.

Each phz molecule has the same geometry as does the free molecule.[50−54] These planar phz molecules are stacked along the *c* axis perpendicular to the [M(CA)(H$_2$O)$_2$]$_k$ chains (nearest neighbor N−C(4″) distance: 3.235(4) Å (**2a**), 3.216(6) Å (**2b**), and 3.263(5) Å (**2c**)), and the plane tilts to the stacking direction by 48.2° (**2a**), 48.7° (**2b**), and 48.0° (**2c**), respectively. The stacking phzs are considered to form a segregated column (Figure 2c). The order of the magnitudes for the stacking distances and angles are in accordance with those of the ionic radii and the first type of hydrogen bond distances as mentioned above. Therefore, the stacking modes of the guest molecules also affect the sheet and chain structures, and moreover, it is possible to tune the columnar structure by selection of the metals. The stacking distance of each phz is shorter than the distance in graphite and that of free phenazine,[50−54] and neighboring phz molecules in a stack have a bond-over-ring (BOR) arrangement, which is found in all superconducting κ-phase BEDT-TTF salts,[55,56] indicating that there exists a large $\pi-\pi$ interaction between phz molecules. In conclusion, the {[M(CA)(H$_2$O)$_2$]$_k$}$_l$ sheet is a common structural motif for new layered materials, which could intercalate functional molecules.

Magnetic Properties. The compounds **1a**−**c** and **2a**−**c** were also obtained as a polycrystalline phase. The powder diffraction patterns of the complexes are in good agreement with those obtained from the single-crystal data. The powder patterns give direct evidence of a single phase in each of the polycrystalline powders.

The ^{57}Fe Mössbauer spectra of **1a** and **2a** (Figure S-1)[77] consist of a single quadrupole doublet with IS =

(50) Herbstein, F. H.; Schmidt, G. M. J. *Acta Crystallogr.* **1955**, *8*, 406.
(51) Herbstein, F. H.; Schmidt, G. M. J. *Acta Crystallogr.* **1955**, *8*, 399.
(52) Hirshfeld, F. L.; Schmidt, G. M. J. *J. Chem. Phys.* **1957**, *26*, 923.
(53) Glazer, A. M. *Philos. Trans. R. Soc. London, Ser. A* **1970**, *266*, 593.
(54) Wozniak, K.; Hariuki, B.; Jones, W. *Acta Crystallogr., Sect. C* **1991**, *47*, 1113.
(55) Williams, J. M.; Ferraro, J. R.; Thorn, R. J.; Douglas Carlson, K.; Geiser, U.; Wang, H.-H.; Kini, A. M.; Whangbo, M.-H. *Organic Superconductors*; Prentice Hall: Englewood Cliffs, NJ, 1992.
(56) Reetz, M. T.; Höoger, S.; Harm, K. *Angew. Chem., Int. Ed. Engl.* **1994**, *33*, 181.
(57) *Chemical Mössbauer Spectroscopy*, Herber, R. H., Ed.; Plenum Press: New York, 1984.
(58) Hrynkiewicz, A. Z.; Sawicka, B. D.; Sawicki, J. A. *Phys. Status. Solidi* **1970**, *38*, K111.
(59) Ingalls, R. I. *Phys. Rev.* **1964**, *133*, A787.
(60) Katada, M.; Uchida, Y.; Iwai, K.; Sano, H.; Sakai, H.; Maeda, Y. *Bull. Chem. Soc. Jpn.* **1987**, *60*, 911.
(61) Asamaki, K.; Nakamoto, T.; Kawata, S.; Sano, H.; Katada, M.; Endo, K. *Inorg. Chim. Acta* **1995**, *236*, 155.
(62) Sato, T.; Ambe, F.; Endo, K.; Katada, M.; Maeda, H.; Nakamoto, K.; Sano, H. *J. Am. Chem. Soc.* **1996**, *118*, 3450.
(63) Figgis, B. N.; Lewis, J.; Mabbs, F. E.; Webb, G. A. *J. Chem. Soc.* **1967**, A442.
(64) Fisher, M. E. *Am. J. Phys.* **1964**, *32*, 343.
(65) Kahn, O. *Molecular Magnetism*; VCH Publishers: New York, 1993.

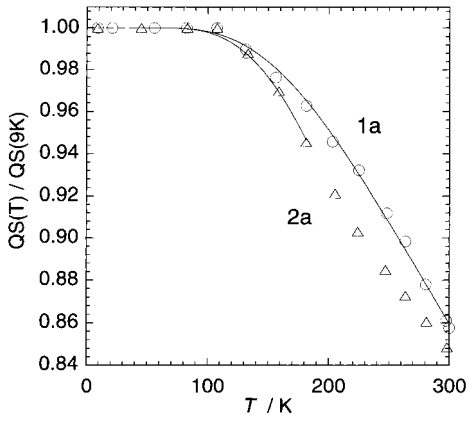

Figure 3. Plots of reduced quadrupole splitting, $QS(T)/QS(9\ K)$ vs T for **1a** and **2a**. Solid lines are the theoretical fits of the data with the parameters listed in the text.

1.16 mm/s (**1a**), 1.16 mm/s (**2a**) and $QS = 2.53$ mm/s (**1a**), 1.46 mm/s (**2a**) at 298 K, respectively, indicating that the oxidation state of the iron in both complexes is two. Although the crystal structure of $[Fe(CA)(H_2O)_2]_n$ is uncertain,[42] the Mössbauer parameters of **1a** are similar to those of $[Fe(CA)(H_2O)_2]_n$, indicative of the similarity of the coordination geometry around the iron. The QS value of **1a** is almost the twice that for **2a**. Normally, if the ligand field potential of **1a** is similar to that of **2a**, the electric field gradient (EFG) of **2a** is twice as large as that of **1a**.[57] On the other hand, the QS value of **2a** is similar to that of $[Fe(C_2O_4)(H_2O)_2]_n$, which has a 1D structure bridged by oxalate and D_{4h} geometry around the iron.[42,47] These features suggest that the intrinsic symmetry around the iron(II) in **1a** is C_{2v} or lower and the rhombic distortion is much larger than that of **2a**. The temperature dependence of the QS of **1a** (Figure 3) shows a gradual decrease with increasing temperature, which may be explained by a low-symmetry crystal field splitting of the $^5T_{2g}$ ground state of octahedral high-spin Fe(II). To calculate the temperature dependence of the QS, we use a three-level scheme, in which the $^5T_{2g}$ ground state is split into A_2, B_1, and B_2 states.[58,59] The thermal distribution of the states follows a Boltzmann distribution as in eq 1, where Δ_1 and Δ_2 are the energy difference between A_2 and B_1 and A_2 and B_2, respectively, and $F(T)$ is proportional to the valence contribution to the EFG tensor. If there is no lattice contribution to the EFG, the QS may be determined according to eq 2.

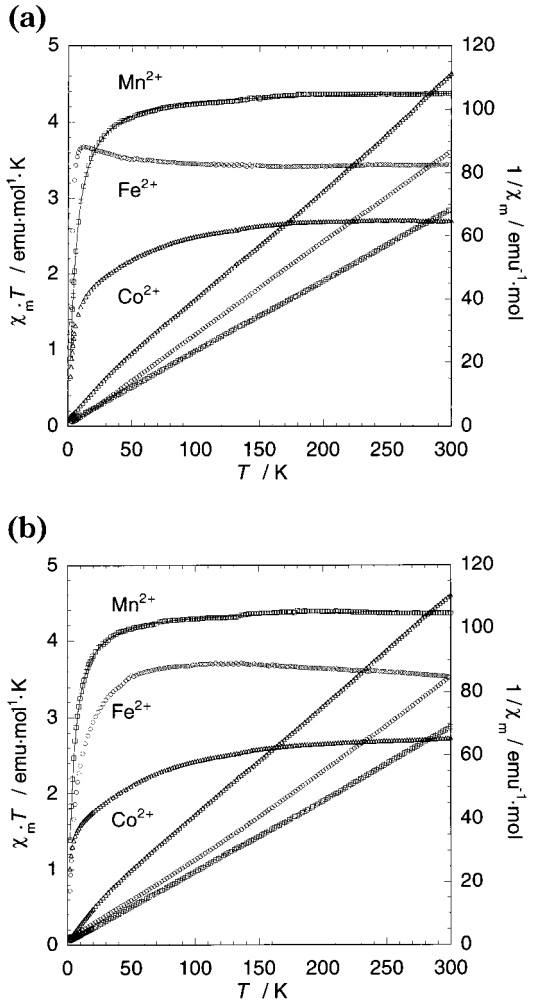

Figure 4. Plots of $\chi_M T$ and $1/\chi_M$ vs T for **1a**−**c** (a) and **2a**−**c** (b). Solid lines: theoretical fits of the data with the parameters listed in the text.

$$F(T) = [[1 + \exp(-2\Delta_1/kT) + \exp(-2\Delta_2/kT) - \exp(-\Delta_1/kT) - \exp(-\Delta_2/kT) - \exp(-(\Delta_1 + \Delta_2)/kT)]^{1/2}]/[1 + \exp(-\Delta_1/kT) + \exp(-\Delta_2/kT)] \quad (1)$$

$$F(T) = QS(T)/QS(0\ K)\ (2) \quad (2)$$

In Figure 4 we have approximated the 0 K value of the QS by using the value determined at 9 K. The temperature variation is fitted with $\Delta_1 = 470\ cm^{-1}$ and $\Delta_2 = 1300\ cm^{-1}$.

On the other hand, the temperature dependence of the QS of **2a** resembles those of $[Fe(C_2O_4)(H_2O)_2]_n$ and $[Fe(C_4O_4)(H_2O)_2]_n$,[42] which are explained by a tetragonal distortion of the $^5T_{2g}$ ground state of octahedral high-spin Fe(II). The $^5T_{2g}$ ground term is split into two terms, ^5E_g and $^5B_{2g}$, by the tetragonal distortion, and **2a** appears to have D_{4h} symmetry around the iron. Thus the temperature dependence of the QS for **2a** is also explained by the same scheme as seen in the case of $[Fe(C_4O_4)(H_2O)_2]_n$ (eq 3).[42]

$$F(T) = QS(T)/QS(0\ K) = \frac{1 - \exp(-\Delta/kT)}{2 + \exp(-\Delta/kT)} \quad (3)$$

The obtained value for the energy difference between the two states is 503 cm^{-1}, assuming a orbitally non-

(66) Bencini, A.; Gatteschi, D. *EPR of Exchange Coupled Systems*; Springer-Verlag: Berlin, 1990.
(67) Deguenon, D.; Bernardinelli, G.; Tuchagues, J.-P.; Castan, P. *Inorg. Chem.* **1990**, *29*, 3031.
(68) Zheng, L.; Schmalle, H. W.; Huber, R.; Decurtins, S. *Polyhedron* **1996**, *15*, 4399.
(69) Verdaguer, M.; Michalowicz, A.; Girerd, J. J.; Alberding, N.; Kahn, O. *Inorg. Chem.* **1980**, *19*, 3271.
(70) Lines, M. E. *J. Chem. Phys* **1971**, *55*, 2977.
(71) De Munno, G.; Julve, M.; Lloret, F.; Faus, J.; Caneschi, A. *J. Chem. Soc., Dalton Trans.* **1994**, 1175.
(72) Kawata, S.; Kitagawa, S.; Furuchi, I.; Kudo, C.; Kamesaki, H.; Kondo, M.; Katada, M.; Munakata, M. *Mol. Cryst. Liq. Cryst.* **1995**, *274*, 179.
(73) Wright, J. D. *Molecular Crystals*, 2nd ed.; Cambridge University Press: Cambridge, U.K., 1995.
(74) Gibb, T. C.; Greenwood, N. N.; Sastry, M. D. *J. Chem. Soc.* **1972**, 1947.
(75) Nicolini, C.; Reiff, W. M. *Inorg. Chim. Acta* **1983**, *68*, 55.
(76) Katada, M.; Yoneyama, M.; Nakai, S.; Kawata, S.; Sano, H. *Hyperfine Interact.* **1994**, *93*, 1477.
(77) Supporting Information.

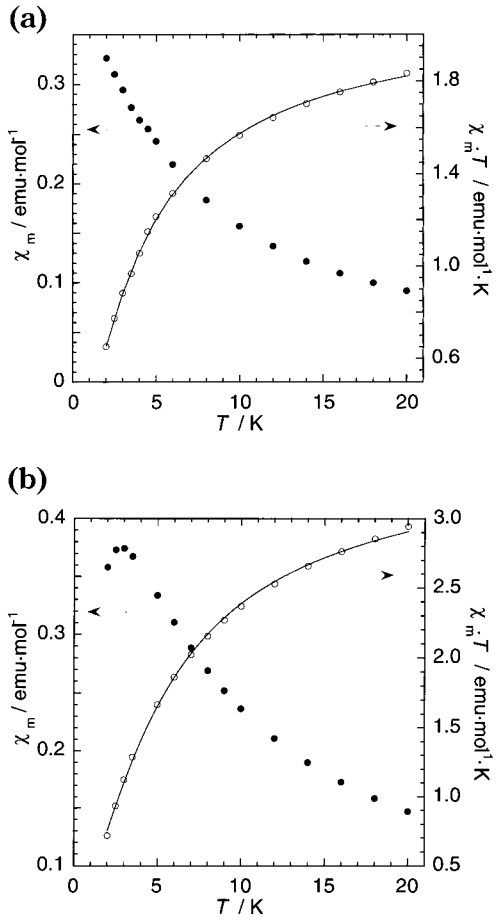

Figure 5. Thermal dependence of $\chi_M T$ for **1b** (a) and **2a** (b) at lower temperature. Solid lines: theoretical fits of the data with the parameters listed in the text.

degenerate $^5B_{2g}$ ground term. This energy splitting is in substantial agreement with the ground term splitting derived from the temperature dependence of the magnetic susceptibility of **2a**. The *QS* values from 9 to 183 K were used for the calculation because of the presence of an inflection around 200 K. Such a discontinuity was also observed in the temperature dependence of the signal intensity which can be replaced for the recoil free fraction, indicative of the existence of a phase transition which is caused by a change of thermal motion of iron atoms in the chain (vide infra).[60−62] However, no discrepancies in the temperature dependence of the magnetic susceptibility of **2a** were observed.

The $\chi_M T$ value of **2a** shows a broad maximum at around 100 K (Figure 4). This behavior is typical of tetragonally distorted Fe(II) in which the high-temperature susceptibility is dominated by a Boltzmann distribution between two terms separated by about 400−700 cm^{-1},[63] which is consistent with the Mössbauer spectral results. At lower temperature $\chi_M T$ decreases in a manner indicative of antiferromagnetic ordering. We have attempted to theoretically reproduce the essential features of the experimental susceptibility of **2a** from 2 to 20 K (Figure 5).[41,42] The data were analyzed by using the infinite chain of classical spins approach (eq 4) derived by Fisher,[41,64,65] to give a fitting with $J = -0.47$ cm^{-1}, $g = 2.26$, and $\rho = 4.4\%$. The observed J value is the same order of magnitude as that of **2c** and can be compared with those of $[Fe(CA)(H_2O)_2]_n$ ($J = -0.1$ cm^{-1}) and $[Fe(DHBQ)(H_2O)_2]_n$ ($J = -1.35$ cm^{-1}).[41,42]

$$\chi = (1-\rho)\frac{2N\beta^2 g^2}{kT} \times \left(\frac{1+\coth(2S(S+1)/kT - kT/2S(S+1))}{1-\coth(2S(S+1)/kT + kT/2S(S+1))}\right) + \frac{\rho N\beta^2 g^2 S(S+1)}{3kT} \quad (4)$$

These features show that the high-spin ions exhibit a weak intrachain antiferromagnetic exchange interaction through chloranilate. On the other hand, the $\chi_M T$ value of **1a** exhibits a minimum but an increase (10−100 K, $\theta = 1.02$ K) and a rapid decreases (2−10 K) at lower temperature indicative of a complicated exchange interaction. However, the origin of the exchange interaction is not clear at this stage because a simple antiferromagnetic interaction is operative for **1b**,**1c** which are isomorphous with **1a** (vide infra).

The $\chi_M T$ in the manganese and cobalt complexes decreases at lower temperature, indicative of antiferromagnetic exchange coupling, leading to a singlet ground state (Figure 4). The temperature variation of the $\chi_M T$ for the manganese complexes were analyzed by using the infinite chain of classical spins approach, to give a fitting with $J = -0.74$ cm^{-1}, $g = 2.01$, $\rho = 1.4\%$ (**1c**) and $J = -0.65$ cm^{-1}, $g = 2.02$, $\rho = 9.0\%$ (**2c**). The g values are consistent with the powder EPR results shown in Figure S-2.[77] The obtained g values are 2.015 (**1c**) and 2.020 (**2c**). The signals around the $\Delta M_s = 1$ region have sharp line widths, and the $\Delta M_s = 2$ absorption[66] was observed for both cases, indicative of the existence of a spin-exchange interaction in the chains as discussed in the cases of $[Mn(bipy)(C_2O_4)]_n$[67] and $\{[Cu(CA)(H_2O)_2](Guest)\}_n$.[6] The obtained J values for **1c** and **2c** are similar to each other whereas the chain structures of them are different. The high-spin manganese(II) ion in an octahedral environment has a ground state, $^6A_{1g}$, which is the totally symmetric representation without first-order orbital momentum. In such a case, the linking geometry in the chain may not efficiently affect the exchange interaction. However, the obtained $|J|$ values are higher than that of $[Mn(CA)(bpy)]_n$[68] which consists of zigzag chains of manganese bridged by chloranilate and terminal bpy, whereas the Mn−Mn distance of $[Mn(CA)(bpy)]_n$ (8.142 Å) in the chain is very close to those of **1c** and **2c**. This discrepancy could arise from difference in the strength of the basicity between H_2O and bpy. The basicity of the terminal ligands would modify the residual spin densities on the bridging chloranilate and hence the magnitude of the intrachain coupling.[6,69]

The $\chi_M T$ value of the cobalt complexes in the higher temperature region are about 2.7, which is larger than the spin only value for $S = 3/2$ (1.876). These behaviors are typical of the Co(II) ion in a distorted octahedral environment, and a large orbital contribution to the magnetic moment should be considered.[70,71] However, at lower temperature the $\chi_M T$ values dramatically decrease in a manner indicative of antiferromagnetic ordering. Thus we have also attempted to fit the essential features of the experimental susceptibility of **1b** from 2 to 20 K by using the simple classical spin approach, to give a fitting with $J = -0.45$ cm^{-1}, $g = 2.10$, and $\rho = 6.6\%$ (Figure 5). On the other hand, we were not able to fit the essential features of **2b** by doing

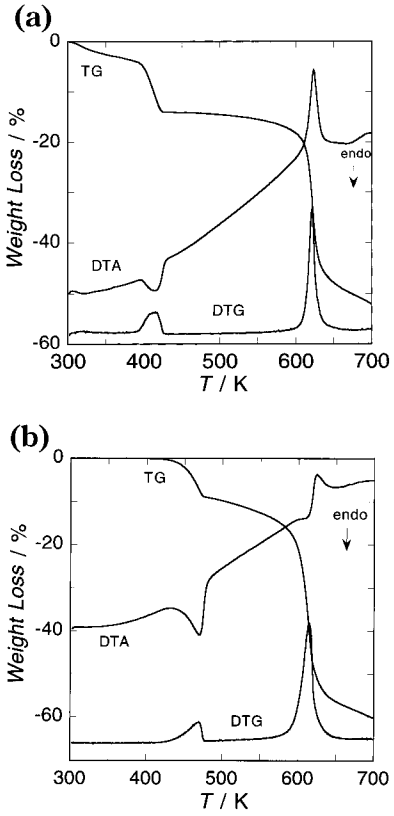

Figure 6. Thermogravimetric analyses data for **1a** (a) and **2a** (b).

the same procedure as described above. It may be because the distortion of the octahedral symmetry of Co(II) ion in **2b** is smaller than that in **1b**.

Thermal Properties of 1a and 2a. To make the host−guest interaction of **1a** and **2a** clear, the TG and DSC measurements have been carried out under a nitrogen atmosphere. The TG diagrams are given in Figure 6. A rapid weight loss takes place up to 430 K for **1a** and 480 K for **2a**, respectively. The liberation of water molecules accounts for these weight losses for **1a** ($3H_2O$, 17%) and **2a** ($2H_2O$, 8.1%).[6,41,42,72] The obtained black species for **1a** in the intermediate range, 430−550 K, is thus assigned to the binary compound $[Fe(CA)]_n$. The Mössbauer spectrum of this product consists of a single quadrupole doublet with $IS = 1.13$ mm/s and $QS = 2.28$ mm/s at 298 K. Although the starting material **1a** shows an EPR signal at around $g = 6$ at 5 K (Figure S-3),[77] $[Fe(CA)]_n$ is EPR silent at room temperature to 5 K, suggesting that an anomalous spin exchange interaction was promoted in the chain. Interestingly, $[Fe(CA)]_n$ is moisture-sensitive and easily changes to $[Fe(CA)(H_2O)_m]_n$, which is confirmed by IR spectroscopy ($\nu_{OH} = 3400$ cm^{-1}). The rehydration process causes the oxidation of the iron center. The Mössbauer spectrum of $[Fe(CA)(H_2O)_m]_n$ consists of a single quadrupole doublet with $IS = 0.37$ mm/s and $QS = 0.39$ mm/s at 298 K (Figure S-4),[77] which shows that the oxidation state of the iron is three.

On the other hand, the obtained species for **2a** in the intermediate range 480−530 K is assigned to $\{[Fe(CA)](phz)\}_n$, and the process of the liberation of water corresponds to eq 5.

This process shows that the coordinated water molecules release easily as compared with the interstitial

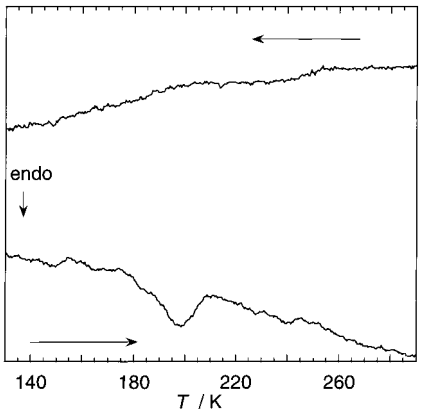

Figure 7. DSC traces of **2a**.

$$\{[Fe(CA)(H_2O)_2](phz)\}_n \rightarrow \{[Fe(CA)](phz)\}_n + 2H_2O \quad (5)$$

organic molecules, indicative of the presence of large reconformation in the crystals. Attempts to generate complexes with cooperative conductive and magnetic properties by solid-state oxidation of **2a** with I_2 at 450 K gave a black powder with $\sigma_{300} \sim 10^{-3}$/S cm^{-1}. The electrical conductivity of **2a** is much less than 10^{-8}/S cm^{-1}. It is clear that the enhanced electrical conductivity of the oxidized polymer is associated with the oxidized nature of this material, although we cannot determine the oxidation site of **2a** at this stage.

The crystallographic structure implies that, in addition to having hydrogen-bonding support the stacking of an intercalated guest, the phz molecule is important for the columnar structure. Moreover, the Mössbauer spectral results show that molecular motion causes a phase transition of **2a** at about 200 K. It is worthwhile to examine the thermal behavior in the lower temperature region. DSC traces of **2a** shows one thermal anomaly at 200 K upon heating indicative of the presence of a phase transition which involves a first-order character (Figure 7). The origin of the phase transition is not clear at this stage. However, reorientation or displacement of the intercalated phz molecules may moderate the phase transition as seen in many molecular crystals[73] and cause the inflection of Mössbauer spectral intensities at around 200 K through a hydrogen-bonding interaction.[74−76]

Conclusions

In this study, we have synthesized a series of layered metal(II) coordination polymers which are supported by a hydrogen-bonding interaction. They are in the category of intercalation compounds. The host layers are classified into two groups: The first type sheet is constructed by zigzag chains (type I), and the second one is formed by straight chains (type II).

The molecular assemblies of metal(II)−CA^{2-} chains and guest molecules obtained here reveal three key factors that control the crystal structures. The first point is the construction of a hydrogen bond-supported 2D sheet, $\{[M(CA)(H_2O)_2]_k\}_l$, which is so flexible and amenable to intercalation of various kinds of molecules by using the hydrogen-bonding interaction. The second point is that the intercalated guest molecules affect the sheet structure and dynamics of $\{[M(CA)(H_2O)_2]_k\}_l$. The

hydrogen bonding increases the dimensionality of the system and thus provides structural varieties in the crystal structure. The third point is that the selection of the metal mediates the fine-tuning of the sheet structure and the conformation of the guest molecules.

The present results also have shown that the metal−CA^{2-} chain is redox active and the CA^{2-} anion behaves as an innocent ligand, which can induce anomalous magnetic and electrical properties when coupled to the metal ions. It is possible to build novel molecular based layered compounds with unique functions by using this kind of ligand.

These results make the structural and material chemistry of transition metal−chloranilate compounds potentially fruitful.

Acknowledgment. This research was supported by a Grant-in-Aid for Scientific Research (No. 09874146) from the Ministry of Education, Science, Sports, and Culture of Japan and the Sumitomo Foundation (No. 970639).

Supporting Information Available: Tables of X-ray data and figures of Mössbauer and thermal data (23 pages); observed and calculated structure factors (24 pages). Ordering information is given on any current masthead page.

CM980326V